

Out-of-Time-Order Correlation at a Quantum Phase Transition

Huitao Shen,^{1,2} Pengfei Zhang,¹ Ruihua Fan,^{1,3} and Hui Zhai^{1,4}

¹*Institute for Advanced Study, Tsinghua University, Beijing, 100084, China*

²*Department of physics, Massachusetts Institute of Technology, Cambridge, MA 02139, USA*

³*Department of Physics, Peking University, Beijing, 100871, China*

⁴*Collaborative Innovation Center of Quantum Matter, Beijing, 100084, China*

(Dated: September 4, 2022)

In this paper we numerically calculate the out-of-time-order correlation functions in the one-dimensional Bose-Hubbard model. Our study is motivated by the conjecture that a system with Lyapunov exponent saturating the upper bound $2\pi/\beta$ will have a holographic dual to a black hole at finite temperature. We further conjecture that for a many-body quantum system with a quantum phase transition, the Lyapunov exponent will have a peak in the quantum critical region where there exists an emergent conformal symmetry and is absent of well-defined quasi-particles. With the help of a relation between the Rényi entropy and the out-of-time-order correlation function, we argue that the out-of-time-order correlation function of the Bose-Hubbard model will also exhibit an exponential behavior at the scrambling time. By fitting the numerical results with an exponential function, we extract the Lyapunov exponents in the one-dimensional Bose-Hubbard model across the quantum critical regime at finite temperature. Our results on the Bose-Hubbard model support the conjecture. We also compute the butterfly velocity and propose how the echo type measurement of this correlator in the cold atom realizations of the Bose-Hubbard model without inverting the Hamiltonian.

I. INTRODUCTION

Recently there is an increasing interest on the out-of-time-order correlation functions (OTOC)^{1–23} defined as

$$F(t) = \langle \hat{W}^\dagger(t) \hat{V}^\dagger(0) \hat{W}(t) \hat{V}(0) \rangle_\beta, \quad (1)$$

where \hat{W} and \hat{V} are normally chosen at local operators. $\hat{W}(t) = e^{i\hat{H}t} \hat{W} e^{-i\hat{H}t}$ and $\langle \dots \rangle_\beta$ denotes a thermal average at temperature $1/\beta = k_B T$. Intuitively, this correlation function can be considered as an overlap of two states $\langle y|x \rangle$, where $|x\rangle = \hat{W}(t) \hat{V}(0)|\beta\rangle$ and $|y\rangle = \hat{V}(0) \hat{W}(t)|\beta\rangle$. $|\beta\rangle$ is the thermofield double state defined as $|\beta\rangle \equiv \sum_n e^{-\beta E_n/2} / \sqrt{Z} |n\rangle |\tilde{n}\rangle$ ²⁴, where $Z = \text{tr} e^{-\beta H}$. $|n\rangle$ and $|\tilde{n}\rangle$ are the corresponding energy eigenstates of the Hamiltonian but in different Hilbert spaces. In this sense, the inner product $\langle y|x \rangle$ measures the difference in the outcome when exchanging the order of two operations $\hat{V}(0)$ and $\hat{W}(t)$. Consider a normalized OTOC

$$\tilde{F}(t) = \frac{\langle y|x \rangle}{\sqrt{\langle x|x \rangle \langle y|y \rangle}}, \quad (2)$$

the exponential deviation of this correlator from unity diagnoses the chaotic behavior and the so-called the “butterfly effect” in a quantum many-body system^{2–12}. More explicitly, if $\tilde{F}(t)$ deviates exponentially as $\alpha_0 - \alpha_1 e^{\lambda_L(t-t_0)}$ starting from t_0 (where $\alpha_0 \approx 1$), and λ_L defines the Lyapunov exponent for this quantum system.

It turns out that the same correlator has emerged in the gravity physics, in the context of which it describes a bulk scattering near the horizon and characterizes the information scrambling^{2–6}. More interestingly, it is shown recently that for quantum systems, the Lyapunov exponent is always bounded by $2\pi/\beta$ ⁹. If a quantum many-body system has an exact holographic dual

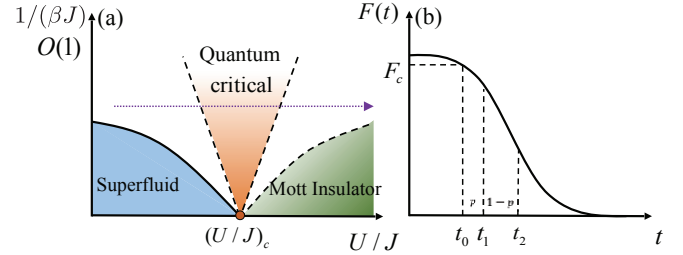


FIG. 1. (a) Schematic of the phase diagram of the Bose-Hubbard model. The dotted line illustrates the parameter regime of the BHM we considered in this work. (b) Schematic of the OTOC and the fitting scheme to obtain the Lyapunov exponent. See the main text for more details on the fitting scheme.

to a black hole at finite temperature^{25–27}, it will have $\lambda_L = 2\pi/\beta$. While a more nontrivial speculation is that if the Lyapunov exponent of a quantum system saturates this bound, this system displays a holographic dual to a black hole⁹. In this sense, the Lyapunov exponent defined in this way measures how close a quantum many-body system is to have a holographic dual. A quantum mechanical model, which is now known as the “Sachdev-Ye-Kitaev” model^{13,28}, has been shown to have emergent conformal symmetry^{13,14,28,29} and the gravitational dual^{15–18}. The OTOC can be calculated explicitly in this model and the Lyapunov exponent is found to saturate the bound^{13,14,19}.

In this work we are interested in studying the OTOC for more realistic models. We will mainly focus on the Bose-Hubbard model (BHM). This model has been well-studied as a text-book example for quantum phase transition after it was proposed in 1989^{30,31}, and since 2011, this model has been realized in cold atom system with

optical lattices and has become one of the most well-studied models experimentally in cold atom physics^{32–34}. The Hamiltonian of the BHM is given by

$$\hat{H} = -J \sum_{\langle ij \rangle} (\hat{b}_i^\dagger \hat{b}_j + \text{h.c.}) + \frac{U}{2} \sum_i \hat{n}_i (\hat{n}_i - 1), \quad (3)$$

where \hat{b}_i is the spinless boson operator at site- i and $\hat{n}_i = \hat{b}_i^\dagger \hat{b}_i$ is the boson number operator. At integer filling, as U/J increases, this model exhibits a quantum phase transition from the superfluid phase to the Mott insulator phase. Fig. 1(a) is a phase diagram for the BHM^{31,35}. Since there is also an emergent conformal symmetry near the critical point, and the quantum critical region is so strongly interacting that there are no well-defined single-particle excitations, it is believed that a (2+1)-dimensional BHM at the quantum critical regime is dual to a gravity model in 4-dimensional Anti-de Sitter space AdS_4 ^{36,37}. Motivated by this argument and the aforementioned insight from the recent studies of the OTOC, we present a *QCP Conjecture* for the Lyapunov exponent that *the Lyapunov exponent will display a maximum around the quantum critical region*. In the BHM, we will consider increasing U/J across the quantum critical regime with a temperature higher than the superfluid transition temperature, as shown by the dotted line in Fig. 1(a).

Hereafter we present a calculation to support this conjecture. Due to the lack of a general effective scheme to calculate the OTOC in the strongly interacting case, we perform an exact diagonalization calculation, in which we first obtain all eigenstates for this many-body system and then compute the time-evolution under the bases of these eigenstates. The calculation is limited to a one-dimensional BHM up to 7 sites. In fact, this is not an ideal situation to demonstrate this conjecture, because, on the one hand, the results suffer from the finite-size effect. On the other hand, the original proposal of the holographic duality is for a (2 + 1)-dimensional BHM. Nevertheless, as we will see, the results support our conjecture.

II. EXPONENTIAL BEHAVIOR OF THE OTOC

Before we proceed to discuss how to extract the Lyapunov exponent from the OTOC of the BHM, we should first answer one question, that is, since the BHM is not really a fully chaotic model, whether we should expect an exponential behavior of the OTOC at the scrambling time. In this section we answer this question by using a rigorous relation between the OTOC at equilibrium and the growth of the second Rényi entropy after a local quench we proved in Ref.³⁸. We will show, by both the numerical calculation and the conformal field theory (CFT) analysis, the second Rényi entropy will grow linearly in time after a local quench at finite temperature, which will imply an exponential behavior of the OTOC.

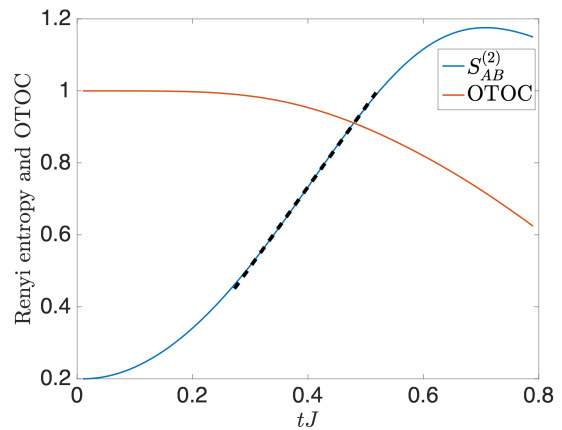


FIG. 2. The growth of the second Rényi entropy $S_A^{(2)}$ and the normalized OTOC as functions of time tJ for $U/J = 10$ at $\beta J = 0.9$ and $N = L = 6$. The linear growth regime of $S_A^{(2)}$ is indicated by a fitted dashed black line.

The theorem between the OTOC and the Rényi entropy states as follows: considering an equilibrium system at temperature T described by density matrix $\rho = e^{-\beta \hat{H}}$, when it is quenched by an operator \hat{O} at time $t = 0$, the density matrix becomes proportional to $\hat{O} \rho \hat{O}^\dagger$ and begin to evolve. We divide the system into two subsystems as A and B , and the second Rényi entropy is defined as $S_A^{(2)} = -\log(\text{Tr} \rho_A^2)$. In Ref.³⁸, we show that this Rényi entropy is related to a modified OTOC function at temperature $T/2$ via:

$$\exp(-S_A^{(2)}) = \sum_{W \in B} \text{tr} \left[\hat{W}^\dagger(t) \hat{O} e^{-\beta \hat{H}} \hat{O}^\dagger \hat{W}(t) \hat{O} e^{-\beta \hat{H}} \hat{O}^\dagger \right], \quad (4)$$

where the summation over \hat{W} is taken over the complete set of operators in system B .

Thus, we can use the behavior of $S_A^{(2)}$ after quench to refer the general behavior of the OTOC under the following two conditions, that are (i) for long time $t \gg \beta$ each term in the R.H.S. of Eq. 4 approaches the OTOC $\text{tr} \left[e^{-2\beta \hat{H}} \hat{W}^\dagger(t) \hat{O} \hat{O}^\dagger \hat{W}(t) \hat{O} \hat{O}^\dagger \right]$ ^{9,23} and (ii) different terms in the summation of the R.H.S. of Eq. 4 have similar function form behaviors. In the rest of this section we will show that during certain time interval after a local quench, $S_A^{(2)}$ will increase linearly as time t , and because of Eq. 4, this indicates an exponential decreasing of OTOC.

To study the entropy growth after a local quench for the 1-D BHM, we firstly use exact diagonalisation method to numerically calculate the second Rényi entropy of a 6-site chain. Here we consider a quench that removes a boson at the third site, which corresponds to a quench operator \hat{b}_3 . Then we divide the system into two equal halves in order to calculate the second Rényi entropy. The result of $S_A^{(2)}$ is shown in Fig 2, which clearly

exhibits a regime with linear growth in time t . For comparison, we also plot an OTOC with the same setup. For the OTOC, we take $\hat{W} = \hat{b}_3$ and $\hat{V} = \hat{b}_4$. Clearly, it is during this time interval of linear growth that the OTOC starts to deviate from unity. In this sense, the linear growth of the second Rényi entropy implies an exponential behavior of the OTOC.

In fact, specifically for this kind of one-dimensional model that can be described by a CFT, the linear growth of the entropy after a local quench can be obtained with a CFT analysis. Considering two half-infinite subsystems A and B at equilibrium at temperature T , in the CFT analysis we mimic a local quench by joining them into a whole system at $t = 0$. To get the Rényi entropy, we need the reduced density matrix for system B at t as

$$\hat{\rho}_A = \text{Tr}_B \left[\exp(-i\hat{H}t) \exp(-\beta\hat{H}') \exp(i\hat{H}t) \right], \quad (5)$$

where \hat{H}' is the Hamiltonian for separated A and B , while \hat{H} is the Hamiltonian for jointed A and B . To using the CFT, instead of real-time, we choose an imaginary-time formalism by analytical continuation³⁹:

$$\hat{\rho}_A = \text{Tr}_B \left[\exp(-\hat{H}(\epsilon + \tau_0)) \exp(-\beta\hat{H}') \exp(-\hat{H}(\epsilon - \tau_0)) \right]. \quad (6)$$

Here we have added a regularization ϵ which should be take to be zero at last. Following the treatment in Ref.³⁹, introducing n replicas and the twist field $\mathcal{T}_n(z)$, one can reduce the problem to the calculation of a single-point correlation function on a manifold with a boundary (see Appendix). The difference is that for our case we consider a system with finite temperature which means our CFT is on a stripe, while in Ref.³⁹ they set $T = 0$ which make their manifold the full plane. The final result in our case is

$$S_A^{(2)} = \frac{c}{8} \log(\sinh(\pi T t)) + \text{constant}, \quad (7)$$

and the long time behavior is given by

$$S_A^{(2)} \sim \frac{c\pi T t}{8}, \quad (8)$$

which demonstrates that the second Rényi entropy growth linearly, and in turn indicates the exponential behavior of the OTOC.

III. THE LYAPUNOV EXPONENT

Now we are in the position to extract the Lyapunov exponent. Three typical curves of the OTOC are shown in Fig. 3(a). In order to fit an exponential deviation behavior for the early period and to obtain a Lyapunov exponent, we adapt the fitting scheme as shown in Fig. 1(b):

1. We choose a threshold F_c ($F_c \lesssim 1$) to determine a starting time t_0 , with $\tilde{F}(t_0) = F_c$. We take t_0 as the initial time that the OTOC starts to deviate exponentially.
2. We take the second-order derivative of $\tilde{F}(t)$, denoted by $\tilde{F}''(t)$, and take t_2 to be the last point (after t_0) that satisfies $\tilde{F}''(t) < 0$. In another word, for $t > t_2$, $\tilde{F}''(t) > 0$ and obviously $\tilde{F}(t)$ can no longer be fitted with an exponential.
3. Even within $t_0 < t < t_2$, not all data points obey the exponential behavior. In fact, the OTOC deviates from the exponential function before reaching t_2 . Therefore we introduce another parameter p , which we call retaining fraction. Assuming all data points are uniformly taken along the time direction, we define t_1 as $t_0 < t_1 < t_2$ and $(t_1 - t_0)/(t_2 - t_0) = p$. The principle of choosing p is to set p as large as possible as long as the error of the fitting is small.
4. We fit all the data in the regime $t_0 < t < t_1$ by a function $f(t) = Ae^{\lambda_L t} + B$. We take the logarithm of the derivative of $f(t)$ as

$$\log(f'(t)) = \log(A\lambda_L e^{\lambda_L t}) = \log(A\lambda_L) + \lambda_L t, \quad (9)$$

where the Lyapunov exponent λ_L can be obtained by the slope of this linear regression.

Before presenting our results, we would like to comment on the separation of time scales in our calculation. There are two time scales involved: the dissipation time t_d and the scrambling time t_s ⁹. They can be extracted from the normal time-order correlators and the OTOC, respectively. Roughly speaking, t_d characterizes the time when the excitation $\hat{V}(0)|\beta\rangle$ is smeared out, so the normal time-ordered correlator factorizes as $\langle \hat{V}^\dagger(0)\hat{W}^\dagger(t)\hat{W}(t)\hat{V}(0) \rangle = \langle \hat{V}^\dagger\hat{V} \rangle \langle \hat{W}^\dagger\hat{W} \rangle$. The scrambling time t_s characterizes the time when the information is scrambled and is identified when $\tilde{F}(t)$ first reaches its local minimum. In order for the physics of scrambling to be well-defined, it requires the separation of time scale, i.e., the scrambling takes place at $t_d \ll t < t_s$. This usually requires a large number of degrees of freedom. Here we do calculate the normal-time-order correlators for the same operators and under the same conditions. We find that, restricted by the system size, there is only a small separation of time scale in the finite-size calculation, despite of how we choose \hat{W} and \hat{V} in the OTOC. We expect that this time scale hierarchy can become clearer when the system size becomes larger.

We first consider the case where \hat{V} and \hat{W} are boson annihilation operators on the same site, as these operators are the most natural local operators in the Bose-Hubbard model. We will later consider boson annihilation operators in the different site and even boson operators in the momentum space.

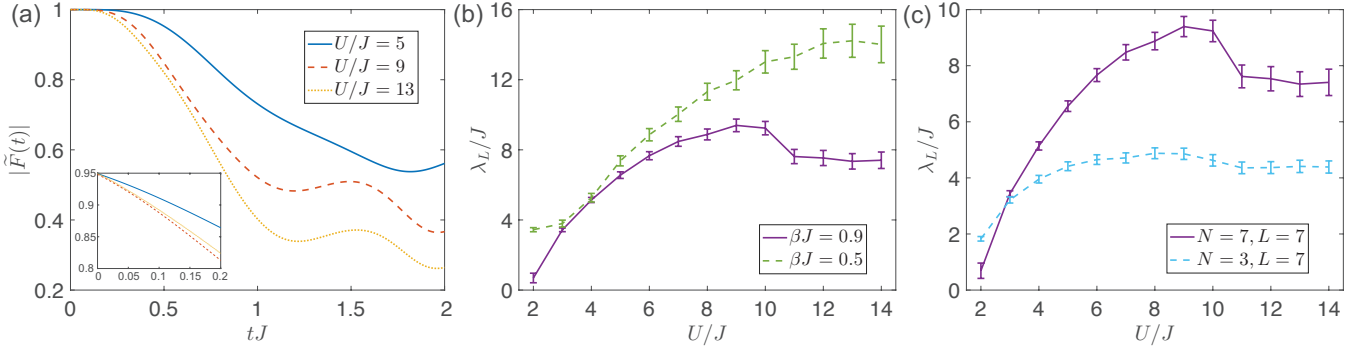


FIG. 3. (a) The amplitude of normalized OTOC $|\tilde{F}(t)|$ as a function of time tJ for $U/J = 5$, $U/J = 9$ and $U/J = 13$ at $\beta J = 0.9$ and $N = L = 7$. The inset is a zoom-in plot of the early-time deviation behavior with t_0 aligned together. It is clear that the $U/J = 9$ curve deviates faster than the $U/J = 5$ and $U/J = 13$ curves. (b-c) The Lyapunov exponents as a function of U/J . The error bars come from the fitting. (b) is plotted for $\beta J = 0.9$ and $\beta J = 0.5$ with $N = L = 7$; (c) is plotted for $N = 7$ and $N = 3$ with $L = 7$, $\beta J = 0.9$. In all the three plots above, we have chosen $\hat{V} = \hat{W} = \hat{b}_1$ and the periodic boundary condition. For the fitting, we take the fitting parameters $F_c = 0.99$ and $p = 0.2$. We have verified that changing the fitting parameters will not affect the trend of the data, but will only modify the exponents quantitatively.

As one can see from the inset of Fig. 3(a), we plot all three OTOC curves starting from their corresponding t_0 with $\beta J = 0.9$ and $N = L = 7$ (N is the number of bosons and L is the number of sites), it is clear that the decreasing first becomes faster as U/J increases, (the curve with $U/J = 9$ decreases faster than that with $U/J = 5$,) and then becomes slower as U/J further increases, (the curve with $U/J = 13$ decreases slower than that with $U/J = 9$.) Fitting this region of data with the scheme mentioned above, we obtain the Lyapunov exponents as a function of U/J . We find that for $\beta J = 0.9$, λ_L displays a broad peak around $U/J = 9$, while when the temperature increases, say, for $\beta J = 0.5$, the peak structure disappears. We also compare λ_L with the upper bound $2\pi/\beta$ and find that at high temperature, λ_L is significantly smaller than the upper bound. As the temperature gets lower, it gets close to the bound. At even lower temperature, we also find that λ_L can exceed the bound. We attribute this to the finite-size effect. For one thing, as when the temperature is comparable to the finite-size gap, the finite-size effect becomes quite significant. The low temperature is only well-defined when the temperature is larger than the finite-size gap. For another thing, the proof of the bound on chaos relies heavily on the large hierarchy between the dissipation time t_d and the scrambling time t_{scr}^9 , which is missing in a numerical calculation in such a small system.¹⁹²³

To further demonstrate that the peak comes from the critical phenomenon, we calculate the case with $N = 3$, $L = 7$ for the same temperature and the interaction parameters. In this case, the filling is sufficient far away from the integer filling and is away from the quantum critical region. Indeed, as shown in Fig. 3(c), we find no peak in λ_L as U/J increases. Also, comparing to the case of the integer filling under the same temperature, λ_L is smaller generically.

There is one thing we should notice. For $(1 + 1)$ -

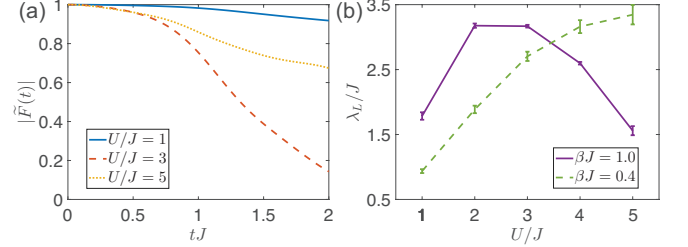


FIG. 4. (a) The amplitude of normalized OTOC $|\tilde{F}(t)|$ as a function of time tJ for $U/J = 1$, $U/J = 3$ and $U/J = 5$ at $\beta J = 1.0$ and $N = L = 6$. (b) The Lyapunov exponents as a function of U/J plotted for $\beta J = 1.0$ and $\beta J = 0.4$ with $N = L = 6$. The error bars come from the fitting. In all the two plots above, we have chosen $\hat{V} = \hat{W} = \hat{b}_k$, $k = \pi/3$ and the periodic boundary condition. For the fitting, we take the fitting parameters $F_c = 0.99$ and $p = 0.8$. We have verified that changing the fitting parameters will not affect the trend of the data, but will only modify the exponents quantitatively.

dimensional BHM, the zero-temperature quantum critical point is located at $U/J \sim 3.4^{40}$, while the peak of λ_L appears at $U/J \sim 9$ in our calculation, which is significantly larger than the zero-temperature critical value. We think this is due to the fact that our calculation is done at a still relatively higher temperature with $\beta J = 0.9$ (further lowering the temperature we will suffer strongly from the finite-size effect and the calculation may not be reliable), and at this temperature the quantum critical region already spans a quite broad area in the parameter space, and perhaps the finite size effect also affects the location of the peak.

In this case we find that the Lyapunov exponent λ_L will also depend on the choice of the operators. Here, instead of the real space boson operator, we can also choose the momentum space boson operator \hat{b}_k as \hat{V} and \hat{W} . Recall

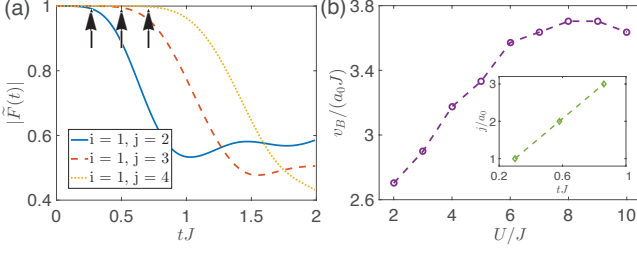


FIG. 5. (a) The amplitude of normalized OTOC $|\tilde{F}(t)|$ as a function of time tJ for $U/J = 6$. $\hat{V} = \hat{b}_i$ and $\hat{W} = \hat{b}_j$ with i fixed at $i = 1$ and j varies between $j = 2$, $j = 3$ and $j = 4$. (b) The butterfly velocity extracted from the OTOC. a_0 is the lattice spacing. The inset is the time t_0 where the OTOC begins to deviate exponentially as a function of the site j for $U/J = 6$. In all the two plots above, we have chosen $\beta J = 0.9$ with $N = L = 7$ and periodic boundary condition. To extract t_0 we choose $F_c = 0.99$.

that we can write the BHM into momentum space as

$$\hat{H} = \sum_{\mathbf{k}} \epsilon_{\mathbf{k}} \hat{b}_{\mathbf{k}}^\dagger \hat{b}_{\mathbf{k}} + \frac{U}{2L} \sum_{\mathbf{k}_1 \mathbf{k}_2 \mathbf{k}_3 \mathbf{k}_4} \hat{b}_{\mathbf{k}_1}^\dagger \hat{b}_{\mathbf{k}_2}^\dagger \hat{b}_{\mathbf{k}_3} \hat{b}_{\mathbf{k}_4}, \quad (10)$$

where $\epsilon_{\mathbf{k}} = 2J \cos k - U/2$ and $\mathbf{k}_1 + \mathbf{k}_2 = \mathbf{k}_3 + \mathbf{k}_4$. Thus $\hat{b}_{\mathbf{k}}$ operator can be regarded as local operator in the momentum space with infinite range interactions. In this case, we find similar behavior of the Lyapunov exponent, as shown in Fig. 4. Nevertheless, we find that the peak of λ_L locates more close to the zero-temperature critical point.

IV. THE BUTTERFLY VELOCITY

Since the BHM we studied here is a model with spatial degrees of freedom and local interactions, we can extract the butterfly velocity from our calculation^{7,41}. For operators with spatial separation $|x|$, the butterfly velocity v_B is defined as $\tilde{F}(t) = \alpha_0 - \alpha_1 e^{\lambda_L(t - |x|/v_B)}$. Let us consider $\hat{V} = \hat{b}_i$ and $\hat{W} = \hat{b}_j$, where i and j are at different sites. t_0 (defined as the time for the onset of the deviation) increases linearly as the distance between i and j , as shown in the Fig. 5(a) and the inset of Fig. 5(b). From this slope we can extract the butterfly velocity and the results are shown in Fig. 5(b). We find the butterfly velocity first increases with U/J . While at large U/J it kind of saturates and even decreases weakly. It is interesting to compare the butterfly velocity with the Lieb-Robinson velocity^{42–44}, which has been studied both theoretically by time-dependent DMRG⁴⁵ and experimentally with cold atoms in optical lattices for the BHM⁴⁶. Since the Lieb-Robinson velocity can somehow be regarded as the butterfly velocity at infinity temperature, it is generally believed that they have the same trend but the butterfly velocity is smaller. This is indeed what we find in our calculation.

V. EXPERIMENTAL OBSERVATION IN COLD ATOM SYSTEM

At last, let us turn to the discussion of experimental measurement of the OTOC in cold atom setting. So far, the existing proposals for measuring OTOC mostly rely on the capability of evolving the system backward in time^{21–23}, that is to say, to invert the entire Hamiltonian from \hat{H} to $-\hat{H}$. We would first remark here that this is doable for cold atom realizations of the BHM. To invert U , one can use the Feshbach resonance to change the sign of the s -wave scattering length. To invert hopping, one needs to use the shaking optical lattice technique. With the Floquet theory, the hopping in a shaken lattice is modified by the zeroth-order Bessel function as $JJ_0(Aa_0m\omega)$, where a_0 is the original lattice space, A is the shaking amplitude, ω is the shaking frequency and m is the mass of atoms. Thus, one can tune the shaking frequency from ω_1 to ω_2 such that $J_0(Aa_0m\omega_1) = -J_0(Aa_0m\omega_2)$. Moreover, there is no intrinsic difficulty that prevents performing these operations simultaneously. Hence, the total Hamiltonian is inverted.

Nevertheless, here we would also like to propose an alternative way to measure OTOC, which does not require inverting the Hamiltonian, but requires preparing two identical copies of the system. This is similar to recent measurement of the second Rényi entropy in the Bose-Hubbard model using a Hong-Ou-Mandel type interference method^{47–49}. Considering an operator $\hat{V} = \hat{O}\hat{O}^\dagger$, similar as discussion above, a modified OTOC is defined as⁹

$$F_M(t) = \text{tr} \left[\hat{W}^\dagger(t) \hat{O} e^{-\beta \hat{H}/2} \hat{O}^\dagger \hat{W}(t) \hat{O} e^{-\beta \hat{H}/2} \hat{O}^\dagger \right]. \quad (11)$$

Recall $\hat{W}(t) = e^{i\hat{H}t} \hat{W} e^{-i\hat{H}t}$, one can show that

$$\begin{aligned} F_M(t) &= \text{tr} \left[e^{i\hat{H}t} \hat{W}^\dagger e^{-i\hat{H}t} \hat{O} e^{-\beta \hat{H}/2} \hat{O}^\dagger e^{i\hat{H}t} \hat{W} e^{-i\hat{H}t} \hat{O} e^{-\beta \hat{H}/2} \hat{O}^\dagger \right] \\ &= \text{tr} [\hat{\rho}_1 \hat{\rho}_2] = \text{tr} [\hat{S}_{12} \hat{\rho}_1 \otimes \hat{\rho}_2], \end{aligned} \quad (12)$$

where

$$\hat{\rho}_1 = \hat{W}^\dagger e^{-i\hat{H}t} \hat{O} e^{-\beta \hat{H}/2} \hat{O}^\dagger e^{i\hat{H}t} \hat{W}, \quad (13)$$

$$\hat{\rho}_2 = e^{-i\hat{H}t} \hat{O} e^{-\beta \hat{H}/2} \hat{O}^\dagger e^{i\hat{H}t}, \quad (14)$$

where we choose a normalization such that $\text{tr}[\hat{\rho}_i] = 1$ and \hat{S}_{12} as a swap operator exchange states of two copies^{48,49}, and allows one to measure $\text{Tr}[\rho_1 \rho_2]$ with the same method as used in Ref.⁴⁹ for measuring the second Rényi entropy.

Thus, to measure the modified OTOC between \hat{W} and $\hat{V} = \hat{O}\hat{O}^\dagger$ at T , the protocol follows from following steps:

1. Prepare two identical copies of the system at $2T$;
2. Apply a sudden quench by applying operator \hat{O} on both system and then let the system evolve under the Hamiltonian \hat{H} by time t

3. Apply an operator \hat{W} only to one of the copies and then measure the interference of the two systems.

In fact, this scheme is closely related to the Loschmidt echo experiment, which has been found recently closely related to the OTOC⁵⁰. The Loschmidt echo experiments have been widely performed in many quantum systems, which can shed light on future investigation of the OTOC.

VI. REMARKS AND THE OUTLOOK

Despite the holographic duality argument, there is also an intuitive argument to understand the peak structure in the Lyapunov exponent. For $U = 0$, the system are non-interacting bosons in a lattice. As U increases, the interaction effect gradually increases λ_L . On the other hand, in the large- U limit, the Hamiltonian and all commutators can be expanded perturbatively in term J/U . For the zeroth order $J/U = 0$, each site becomes independent and the OTOC does not change with time. The Lyapunov exponent λ_L should increase as J/U decreases. Thus we would expect that λ_L has a peak in between.

Therefore, we believe that our *QCP Conjecture* for the Lyapunov exponent can be more general and applies beyond the BHM. In fact, the underlying insight from the condensed matter physics view point is that there are no well-defined quasiparticles in the strongly interacting quantum critical region, and therefore, it is more chaotic

than in the non-critical phase. As a result, the Lyapunov exponent should be larger in this region. For example, we have also studied the quantum phase transition in the XXZ model and the transverse Ising model, where similar phenomena are also found there, although that the integrability of these two models make the situations more subtle. For the XXZ model,

$$\hat{H} = \sum_i J_{\perp} (\hat{s}_i^x \hat{s}_{i+1}^x + \hat{s}_i^y \hat{s}_{i+1}^y) + J_z \hat{s}_i^z \hat{s}_{i+1}^z, \quad (15)$$

where \hat{s}_i^{α} , $\alpha = x, y, z$ are spin operators on site- i . Motivated by the bosonization argument, we choose $\hat{W} = \hat{V} = \hat{s}_i^+ - \hat{s}_{i+1}^+$, whose bosonization representation is the same as that of \hat{b}_i^{\dagger} in BHM. For the transverse Ising model, we have to use the open boundary condition and choose boundary operators in order to characterize the phase transition. In both cases, we find a broad peak of the Lyapunov exponent around the quantum critical region. This conjecture can be tested by more numerical and experimental studies in the future. The OTOC provides an alternative angle to study quantum many-body system, from which more rich physics can be expected.

Acknowledgment. We would like to thank Yingfei Gu and Chao-Ming Jian for helpful discussions. This work is supported by MOST under Grant No. 2016YFA0301600, NSFC Grant No. 11325418 and Tsinghua University Initiative Scientific Research Program.

-
- ¹ A. I. Larkin and Y. N. Ovchinnikov, Sov. Phys. JETP **28**, 1200 (1969).
 - ² S. H. Shenker and D. Stanford, J. High Energy Phys. **2014**, 67 (2014), arXiv:1306.0622.
 - ³ S. H. Shenker and D. Stanford, J. High Energy Phys. **2014**, 46 (2014), arXiv:1312.3296.
 - ⁴ A. Almheiri, D. Marolf, J. Polchinski, D. Stanford, and J. Sully, J. High Energy Phys. **2013**, 18 (2013), arXiv:1304.6483.
 - ⁵ S. H. Shenker and D. Stanford, J. High Energy Phys. **2015**, 132 (2015), arXiv:1412.6087.
 - ⁶ A. Kitaev, "Hidden correlations in the hawking radiation and thermal noise," (2014), a talk given at Fundamental Physics Prize Symposium, 2014.
 - ⁷ D. A. Roberts, D. Stanford, and L. Susskind, J. High Energy Phys. **2015**, 51 (2015), arXiv:1409.8180.
 - ⁸ D. A. Roberts and D. Stanford, Phys. Rev. Lett. **115**, 131603 (2015), arXiv:1412.5123.
 - ⁹ J. Maldacena, S. H. Shenker, and D. Stanford, arXiv:1503.01409.
 - ¹⁰ D. Stanford, arXiv:1512.07687.
 - ¹¹ P. Hosur, X.-L. Qi, D. A. Roberts, and B. Yoshida, J. High Energy Phys. **2016**, 4 (2016), arXiv:1511.04021.
 - ¹² Y. Gu and X.-L. Qi, arXiv:1602.06543.
 - ¹³ A. Kitaev, "A simple model of quantum holography," (2015), a talk given at the KITP Program: Entanglement in Strongly-Correlated Quantum Matter, 2015.
 - ¹⁴ J. Maldacena and D. Stanford, arXiv:1604.07818.
 - ¹⁵ A. Jevicki, K. Suzuki, and J. Yoon, J. High Energy Phys. **2016**, 7 (2016), arXiv:1603.06246.
 - ¹⁶ K. Jensen, arXiv:1605.06098.
 - ¹⁷ J. Maldacena, D. Stanford, and Z. Yang, arXiv:1606.01857.
 - ¹⁸ J. Engelsöy, T. G. Mertens, and H. Verlinde, J. High Energy Phys. **2016**, 139 (2016), arXiv:1606.03438.
 - ¹⁹ W. Fu and S. Sachdev, Phys. Rev. B **94**, 035135 (2016), arXiv:1603.05246.
 - ²⁰ I. Danshita, M. Hanada, and M. Tezuka, arXiv:1606.02454.
 - ²¹ B. Swingle, G. Bentsen, M. Schleier-Smith, and P. Hayden, arXiv:1602.06271.
 - ²² G. Zhu, M. Hafezi, and T. Grover, arXiv:1607.00079.
 - ²³ N. Y. Yao, F. Grusdt, B. Swingle, M. D. Lukin, D. M. Stamper-Kurn, J. E. Moore, and E. A. Demler, arXiv:1607.01801.
 - ²⁴ W. Israel, Phys. Lett. A **57**, 107 (1976).
 - ²⁵ J. M. Maldacena, Int. J. Theor. Phys. **38**, 1113 (1997), arXiv:9711200 [hep-th].
 - ²⁶ E. Witten, Adv. Theor. Math. Phys. **2**, 253 (1998), arXiv:9802150 [hep-th].
 - ²⁷ S. Gubser, I. Klebanov, and A. Polyakov, Phys. Lett. B **428**, 105 (1998), arXiv:9802109 [hep-th].
 - ²⁸ S. Sachdev and J. Ye, Phys. Rev. Lett. **70**, 3339 (1993), arXiv:9212030 [cond-mat].

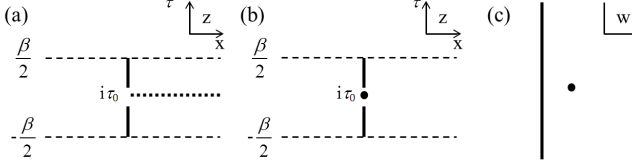


FIG. 6. The procedure of the conformal field theory calculation. (a) The original geometry on the stripe. There is a physical boundary along the imaginary axis and a cut along $+x$ direction from $z = i\tau_0$. For $\text{tr}[\rho^n]$ we need n copies and sew them together. (b) The complicated Riemann surface is identified with a twist field at $z = i\tau_0$ with n copies of field on a single stripe. (c) After conformal mapping, the problem becomes a standard geometry for a half infinite plane.

- ²⁹ O. Parcollet, A. Georges, G. Kotliar, and A. Sengupta, Phys. Rev. B **58**, 3794 (1998), arXiv:9711192 [cond-mat].
- ³⁰ M. P. A. Fisher, P. B. Weichman, G. Grinstein, and D. S. Fisher, Phys. Rev. B **40**, 546 (1989).
- ³¹ S. Sachdev, *Quantum Phase Transitions* (Cambridge University Press, 2011).
- ³² I. Bloch, J. Dalibard, and W. Zwerger, Rev. Mod. Phys. **80**, 885 (2008), arXiv:0704.3011.
- ³³ V. I. Yukalov, Laser Phys. **19**, 1 (2009), arXiv:0901.0636.
- ³⁴ D. Jaksch and P. Zoller, Ann. Phys. (N. Y.) **315**, 52 (2005), arXiv:0410614 [cond-mat].
- ³⁵ Y. Kato, Q. Zhou, N. Kawashima, and N. Trivedi, Nat. Phys. **4**, 617 (2008).
- ³⁶ S. Sachdev, Annu. Rev. Condens. Matter Phys. **3**, 9 (2012), arXiv:1108.1197.
- ³⁷ M. Fujita, S. M. Harrison, A. Karch, R. Meyer, and N. M. Paquette, J. High Energy Phys. **2015**, 68 (2015), arXiv:1411.7899.
- ³⁸ R. Fan, P. Zhang, H. Shen, and H. Zhai, arXiv:1608.01914.
- ³⁹ P. Calabrese and J. Cardy, J. Phys. A Math. Theor. **42**, 504005 (2009), arXiv:0905.4013.
- ⁴⁰ T. D. Kühner, S. R. White, and H. Monien, Phys. Rev. B **61**, 12474 (2000), arXiv:9906019 [cond-mat].
- ⁴¹ D. A. Roberts and B. Swingle, arXiv:1603.09298.
- ⁴² E. H. Lieb and D. W. Robinson, Commun. Math. Phys. **28**, 251 (1972).
- ⁴³ M. B. Hastings and T. Koma, Commun. Math. Phys. **265**, 781 (2006), arXiv:0507008 [math-ph].
- ⁴⁴ B. Nachtergaele and R. Sims, Commun. Math. Phys. **265**, 119 (2006), arXiv:0506030 [math-ph].
- ⁴⁵ A. M. Läuchli and C. Kollath, J. Stat. Mech. Theory Exp. **2008**, P05018 (2008), arXiv:0803.2947.
- ⁴⁶ M. Cheneau, P. Barmettler, D. Poletti, M. Endres, P. Schauss, T. Fukuhara, C. Gross, I. Bloch, C. Kollath, and S. Kuhr, Nature **481**, 484 (2012), arXiv:1111.0776.
- ⁴⁷ C. K. Hong, Z. Y. Ou, and L. Mandel, Phys. Rev. Lett. **59**, 2044 (1987).
- ⁴⁸ A. J. Daley, H. Pichler, J. Schachenmayer, and P. Zoller, Phys. Rev. Lett. **109**, 020505 (2012), arXiv:1205.1521.
- ⁴⁹ R. Islam, R. Ma, P. M. Preiss, M. Eric Tai, A. Lukin, M. Rispoli, and M. Greiner, Nature **528**, 77 (2015), arXiv:1509.01160.
- ⁵⁰ J. Kurchan, arXiv:1612.01278.

Appendix: The Rényi Entropy Growth after a Local Quench: CFT Calculation

In this appendix, we detail the CFT calculation from Eq.(6) to Eq.(7). The technique used here is similar to

Ref.³⁹.

We put our system on a stripe with a periodic boundary along the time direction as shown in Fig. 6(a), the evolution of which is governed by H' . We call the $x > 0$ part A and $x < 0$ part B. And there is no interaction between them. The local quench is achieved by connecting A and B in a small time window ϵ near $i\tau_0$ as shown in Fig. 6(a). We put a cut along space direction at time τ along $+x$ direction because there is no trace over system A. The value of field at the upper (lower) branch of the cut-line gives the Row (column) index of the density matrix $\hat{\rho}_A$.

The calculation of n -th Rényi entropy requires n copies of the stripe. We use the complex coordinate $z = x + i\tau$ for each stripe and sew these stripes one by one by imposing the boundary condition $\phi_{i+1}(x + i\tau_0 + i0^+) = \phi_i(x + i\tau_0 - i0^+)$ for $x > 0$ (the label for copies is defined mod n). Here ϕ is the field contained in the CFT, which is also the label of coherent state for corresponding operator. As a result, the sewed stripes form a complicated Riemann surface. Then we have:

$$\text{tr}[\hat{\rho}_A^n] = \int_{\text{bound.con.}} \mathcal{D}\phi_i \exp(-\sum_i S[\phi_i]).$$

Here $S[\phi]$ is the action for a single copy of field ϕ . Equivalently, we can represent the boundary condition by introducing twist field $\mathcal{T}_n(i\tau_0)$ ³⁹ which act at time τ_0 and swap the value of field to the right of x :

$$\text{tr}[\hat{\rho}_A^n] = \int \mathcal{D}\phi_i \mathcal{T}_n(i\tau_0) \exp(-\sum_i S[\phi_i]).$$

\mathcal{T}_n is known as a primary field with conformal dimension $d_n = \frac{c}{12}(n - \frac{1}{n})$ where c is the central charge. The configuration is shown in Fig. 6(b).

This strip (z) can be mapped to a half infinite plane with a boundary at imaginary axis (w) using conformal transformation:

$$\epsilon w = \tanh \pi z / \beta + \sqrt{\tanh(\pi z / \beta)^2 + \epsilon^2}.$$

The standard formula for the conformal field theory with a boundary⁵⁰ gives the expectation on the stripe shown in Fig. 6(c):

$$\text{tr}[\hat{\rho}_A^n] = \langle \mathcal{T}_n(z) \rangle = c_n \left(\left| \frac{dw}{dz} \right| \frac{1}{2\text{Re}w} \right)^{d_n}, \quad (\text{A.1})$$

where c_n is some constant. Then after the analytical continuation back to the real time and taking cutoff ϵ to zero, one get the result Eq.(7).